Structure-from-Sherds: Incremental 3D Reassembly of Axially Symmetric Pots from Unordered and Mixed Fragment Collections

Je Hyeong Hong*†
KIST, Hanyang University
jhh37@hanyang.ac.kr

Seong Jong Yoo*
KIST
yoosj@kist.re.kr

Muhammad Zeeshan Arshad
KIST
zeeshan@kist.re.kr

Young Min Kim
Seoul National University
youngmin.kim@snu.ac.kr

Jinwook Kim†
KIST
zinook@kist.re.kr

Abstract

Re-assembling multiple pots accurately from numerous 3D scanned fragments remains a challenging task to this date. Previous methods extract all potential matching pairs of pot sherds and considers them simultaneously to search for an optimal global pot configuration. In this work, we empirically show such global approach greatly suffers from false positive matches between sherds inflicted by indistinctive sharp fracture surfaces in pot fragments. To mitigate this problem, we take inspirations from the field of structure-from-motion (SfM), where many pipelines have matured in reconstructing a 3D scene from multiple images. Motivated by the success of the incremental approach in robust SfM, we present an efficient reassembly method for axially symmetric pots based on iterative registration of one sherd at a time. Our method goes beyond replicating incremental SfM and addresses indistinguishable false matches by embracing beam search to explore multitudes of registration possibilities. Additionally, we utilize multiple roots in each step to allow simultaneous reassembly of multiple pots. The proposed approach shows above 80% reassembly accuracy on a dataset of real 80 fragments mixed from 5 pots, pushing the state-of-the-art and paving the way towards the goal of large-scale pot reassembly. Our code and preprocessed data is available at https://github.com/SeongJong-Yoo/structure-from-sherds.

1. Introduction

Ceramic pots are fundamental cultural relics in human history. Most of them are made on a spinning wheel, encompassing axial symmetry. While they provide meaningful information to understanding ancestral lifestyles, many pots are excavated as broken pieces (known as sherds), necessitating accurate reassembly from these sherds for the purpose of recovering historical records.

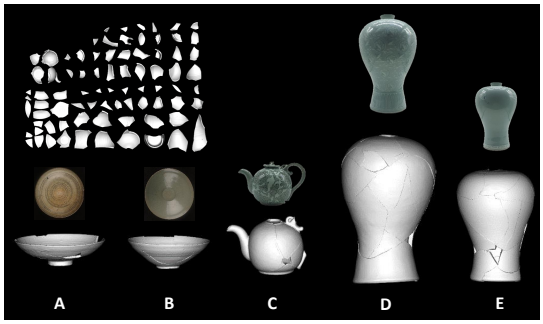

Figure 1. An illustration of 5 real pots simultaneously reassembled from 80 unclustered sherds (3D point clouds) using our pipeline. It can handle some degree of non-axially symmetric decorations on the pot surface as shown in pot C. Ground truth (manually restored) pot images are shown above each reassembly result.

Currently, the process of reassembly is relied upon extensive manual efforts from restoration experts. Despite years of experience, however, reconstructing each pot can often require hours of concentration even for the qualified professionals as fragments are mixed from multiple pots. Furthermore, pieces are fitted on a trial-and-error basis, potentially incurring undesired abrasions on the break surfaces of sherds. These motivate strong need for an efficient framework that can virtually reassemble axially symmetric pots.

Recent studies have proposed pipelines [18, 13] majorly comprising 3 stages, first extracting features from each pot sherd, second computing potential matches between each pair of sherds, and last performing global combinatorial optimization to deduce the most likely 3D pot configuration from these matches. These are known as *global* approaches since the last stage can be viewed as finding true positive sherd matches from the global pot configuration graph. Nevertheless, our effort of implementing such pipeline raises an inherent issue illustrated in Fig. 2, that a

*Both authors contributed equally to this work.
†Co-corresponding authors

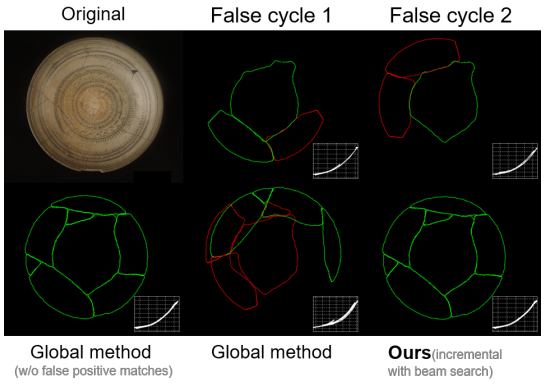

Figure 2. The top row shows some exemplary false positive loops formed in pot A from Fig 1. (True configurations in green and false in red.) Some pairwise matches are difficult to detect even at the cycle level just by looking at the break lines and the axis profile curve (in white). The global method only succeeds when false positive matches are removed. Our incremental method with beam search outputs the correct result in spite of false matches.

global method is sensitive to false positive matches between pot sherds as it directly derives each sherd's configuration from these matches. Unfortunately, such false positives are widespread due to lack of distinctive features on the fracture surfaces as the result of sharply broken edges (see Fig. 3).

In addressing above issue, we turn our attention to structure-from-motion (SfM), which have enjoyed tremendous success over the last few decades in reconstructing 3D scenes from thousands of images [17, 1, 22, 16]. Behind this achievement lies the *incremental* method, which mains robustness to numerous false positive matches by iteratively registering one camera view at a time in descending order of connectivity. The essence of the incremental method lies in its ability to *iteratively improve pairwise matches and discover initially undetected (false negative) matches* as the model grows, which can be tricky for the global approaches that relies on pruning initial pairwise matches only.

A naturally following question is, can we apply the findings from incremental SfM to devise a reliable method for reassembling axially symmetric pots from fragments? As will be illustrated in Sec. 2.2, we find both tasks share a great deal of analogy in terms of the problem and (global) pipeline structures, potentially allowing a smooth transfer of the incremental method from the domain of SfM to pot reassembly. Yet, pot reassembly requires handling additional challenges such as mitigating incorrect sherd registration triggered by many indistinguishable false positive sherd matches (due to ambiguous geometric features) and enabling reassembly of multiple pot models.

To this end, we propose *structure-from-sherds* (SfS), an efficient incremental method for reassembling multiple pots from fragments. Our method follows the iterative sherd registration scheme to grow the reassembly model like in incremental SfM, but some extensions are without which the

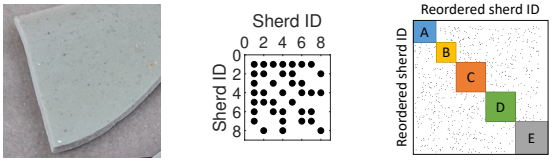

(a) (b) (c)

Figure 3. Illustration of some challenges in reassembling multiple axially symmetric pots. (a) shows sharp, thin fracture surfaces with little distinct features triggering false positive sherd matches. (b) shows the sparse nature of connectivity between sherds from the same pot (59% filled across 8 sherds of pot A in Table 2). (c) illustrates the noisy block-diagonal sparsity structure of the problem when sherds are mixed from different fragments (See Sec. 2.1).

reassembly performance is limited (see Table 3). These include adopting beam search to explore multiple registration possibilities in each step to compensate for indistinguishable false matches, and employing multiple sherd roots in each beam state to reassemble multiple pots simultaneously.

Our main technical contributions are as follows:

+ a **new pot reassembly pipeline** derived from our unification of structure-from-motion and pot reassembly (Sec. 2.2) and based on multi-root beam search, yielding more complete pots from more fragments [18],
+ a **new axis-based geometric descriptor** for the break line points, removing a need to use surface point cloud for efficient initial sherd matching(Sec. 3.4)
+ **simple algorithms** for extracting and utilizing rim, base and thickness to reduce false matches and further improve registration accuracy (Table 3), and
+ a **new challenging dataset** of 80 real pot sherds from 5 different pots made for evaluation (Table 2).

Conversely, our implementation has some limitations: currently, it requires at least part of the base fragment for each pot to be correctly reassembled (see Sec. 5.4). Also, we do not utilize fragment texture (like in [18]) because the 3D scanner often fails in stitching the texture correctly and suffers from light saturation. Nonetheless, we believe this work would serve as the basis for further improvements.

1.1. Related work

The problem of virtually reassembling archaeological pots has received consistent attention in computer vision and graphics [12, 8, 20, 18, 24] over the last two decades.

In the early days, several works showed ways to extract geometric properties of the axially symmetric pot from individual fragments such as the axis of symmetry [14, 3, 11] or the profile shape (i.e. axis profile curve) [19]. Mcbride an Kimia [12] devised a method for matching pairs of sherds, and noted this process is much more involved than solving a jigsaw puzzle due to the non-unique break lines.

It was Willis and Cooper [20] who first pioneered a reassembly pipeline for axially symmetric pots. Their method follows an incremental registration procedure like ours,

	Structure-from-motion (SfM)	Pot reassembly
Input	RGB images	3D point cloud of pot sherds
Outputs	camera poses & sparse 3D scene	sherd poses & axially symmetric pot models
Extracted features	SIFT [10] keypoints	axis, edge line descriptor, rim, thickness, base
Pairwise matching criteria	SIFT feature distance	Weighted sum of above features
Geometric verification	inliers from fundamental (or essential) matrix or homography estimation	inliers from iterative closest point (ICP)
Sanity check	cheirality constraint	overlap, thickness & profile curve constraints
Registered quantity	camera views	sherds
Triangulated model	3D scene points	3D pot model (axis of symmetry & profile curve)
Joint estimation	bundle adjustment	global sherd and axis alignment via ICP

Table 1. A list of analogies formed between an incremental structure-from-motion pipeline [16] and our pot reassembly method.

adding each fragment one by one to gradually grow the global consensus of the outputted model. In each step, the best candidate sherd is chosen by considering its matching degree of break line points, the corresponding surface normals and the axis profile curve. Nevertheless, it requires manual effort to extract features known as the T-junctions on the break lines, and has only been tested on a single pot case of 10 sherds. Furthermore, there is no backtracking procedure that avoids failures from incorrect registration.

In later years, Son et al. [18] presented a type of global approach to tackling the reassembly problem with 48 fragments from 3 pots. The method considers all potential pairwise matches across all pot sherds jointly and solves a combinatorial optimization problem of finding true positive fragment pairs to directly retrieve the 3D pot model. This is carried out by minimizing algebraic costs promoting consistency of the axis of symmetry and the axis profile curve using a spectral method [9]. While the results have demonstrated state-of-the-art performance, it is unclear as to how the false positive matches are handled—they are sometimes indistinguishable from ground truth [20], which can be detrimental for global approaches as shown in Fig. 2.

Other studies include the work of Huang et al. [8], which proposes an incremental method for reassembling geometric objects, but this relies on existence of rich unique features on the break surface which is often not visible in pot sherds (see Fig. 3a). Also, the method has only been tested for reassembling single objects. Zhang et al. [24] presented a template-based matching technique, but this is also limited to single object cases with known pot templates.

2. Devising a robust reassembly pipeline

We now review the challenging aspects of axially symmetric pot reassembly, compare this problem to well-established SfM to gain intuitions for a successful methodology and propose our pipeline for the pot reassembly task.

2.1. Review of problem characteristics

Some main problem characteristics exhibited in reassembling axially symmetric pots are summarized below:

Existence of numerous false positive matches Fig. 3 shows the fracture surface (often used for matching [8, 24]) is thin and sharply broken for ceramic pots. It is therefore difficult to detect features and distinguish between break lines, raising the number of false positive matches.

Sparse intra-pot connectivity For pot reassembly, each sherd pair must be physically adjacent, resulting in a sparse connectivity graph between sherds. This is shown in Fig. 3, where pot A (Fig. 2) contains only 59% filled graph.

Sparse but noisy inter-pot connectivity For multiple pot reassembly, fragments end up in different pots, yielding a block-diagonal pot configuration graph plagued by false positive matches as shown in Fig. 3. This further raises the problem difficulty, and subsequently a reassembly pipeline needs to handle noisy but originally-disconnected graphs. (otherwise one may recover only one pot at best.)

2.2. Comparing axially symmetric pot reassembly with structure-from-motion

We now present an analogy between the task of pot reassembly and structure-from-motion (SfM) that allows us to intuitively derive a similar pipeline for pot reassembly.

Problem analogy Structure-from-motion (SfM) is a multi-stage pipeline jointly estimating 3D scene points and camera poses from a set of input images. We can also think of pot reassembly as jointly estimating a 3D pot model (defined by the axis of symmetry and the axis profile curve) and sherd transformations from 3D point cloud data of sherds. In this regards, both tasks amount to solving an optimization problem over a sparsely connected graph (see Fig. 3).

Procedural similarities There are noticeable similarities between the SfM pipeline and pot reassembly methods.

Regarding the global methods, global SfM proceeds by first extracting features from individual images, second searching for pairwise matches between images, and last pruning these matches via triplet or loop filtering [23] to yield a global model of camera poses and 3D points (involving rotation averaging [4] and translation averaging [21] followed by bundle adjustment [5]). Similarly, Son et al.'s approach [18], which is a type of global pot reassembly method, comprises similar steps, extracting axis-based and

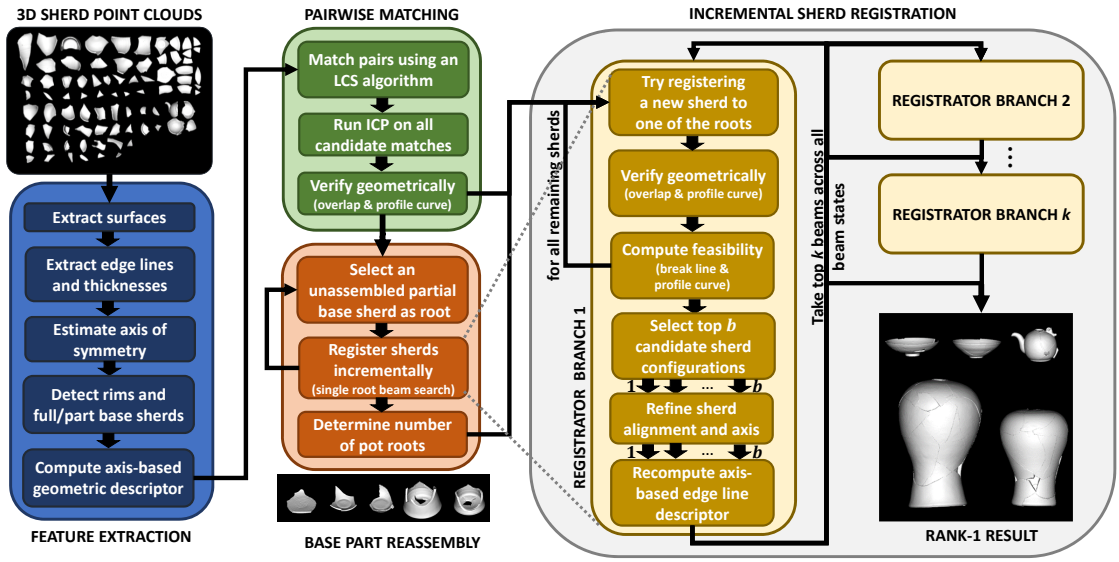

Figure 4. A detailed overview of our pipeline. Multiple arrows $(1, \ldots, b)$ in registrator branch 1 represent multiple branches formed. The grey dotted lines indicate the incremental registration step during base part reassembly has a similar structure to registrator branch 1.

break line-based features for each sherd, searching for pairwise matches between sherds and last solving a graph optimization problem (via spectral method) to find a global pot model (defined by the axis of symmetry and axis profile curve) and respective sherd transformations.

Analogical connections in procedures From the procedural similarities outlined above, we can yield a full list of analogies (see Table 1) formed between SfM and axially symmetric pot reassembly. This enables us to effectively import the architecture of the well-established incremental SfM pipeline to reassembling axially symmetric pots.

Empirical differences As shown in Fig. 2, we have empirically found false positive pairwise matches are highly problematic in pot reassembly as some are almost indistinguishable from the true positives even from the human eye perspective (even after applying false cycle filtering as in [23]). Also, pot reassembly needs to build multiple disconnected models whereas SfM often builds a single scene.

2.3. An overview of the proposed pipeline

Our proposed pipeline for reassembling axially symmetric pots is founded upon the findings from Sec. 2.2.

As shown in Fig. 4, our pipeline is modified and extended from a standard incremental pipeline to achieve more accurate reassembly results in spite of large number of false matches and existence of multiple disconnected pots.

First, the method incorporates beam search during the incremental sherd registration phase, exploring many more paths of possibilites in each step thereby increasing the chance of arriving at the correct solution.

Second, the pipeline efficiently reassembles the base regions first to determine the number of pots to be reconstructed as well as yield a good initial starting point. (A base is the flat region at the bottom of each pot.)

Each pipeline stage is illustrated in the next sections.

3. Feature extraction from individual sherds

We extract features from each sherd, including the inner and outer surfaces and edge line, estimating the axis of symmetry and detecting base and rim parts in each fragment.

3.1. Extracting surfaces and edge lines

We first extract two surfaces corresponding to inner and outer surfaces. (we later use the axis of symmetry to classify between the two surfaces [7].) Then for each of the surfaces, we extract an ordered line of points around the edge of each surface which we defined as an *edge line*. This is essentially a vector of ordered (counter-clockwise) 3D points and respective surface normals on the surface boundary. Rather than storing the actual surface normal of each edge point (which can be noisy due to the fracture surface), we fit a B-spline curve to the surface and compute the estimated normal of the edge point from the curve. This vector is further segmented to different parts, which is later used for detecting rim and break lines (see Fig. 5.)

Additionally, we extract thickness information (t in Fig. 7). Details can be found in our supplementary URL [7].

3.2. Estimating the axis of symmetry

From the analogy in Table 1, estimating the axis of symmetry can be seen as inferring the underlying pot model.

Amongst the algorithms for estimating the axis of symmetry [3, 11, 18, 6], the state-of-the-art performance is achieved by PotSAC [6]. While the original PotSAC is limited to outputting a single axis even for ambiguous sherds,

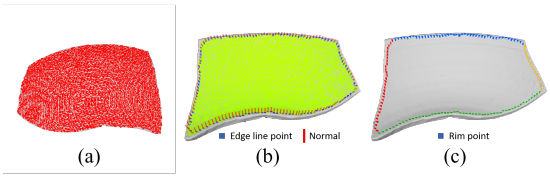

Figure 5. Features extracted in Sec. 3.1. Yellow and red denote inner and outer surfaces. Each edge line along the boundary of the surface contains normals computed from its nearest surface point.

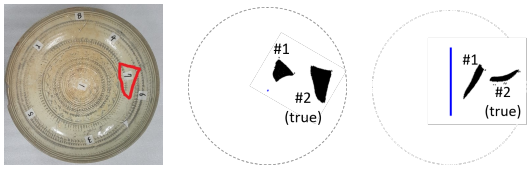

(a) Original image (b) Top view (c) Side view

Figure 6. Axis estimation results using modified PotSAC on sherd #7 from Pot A. Original PotSAC outputs incorrect #1 for the axis.

we present a slight modification that can output multiple axes which allows us to avoid failures for these cases.

The basic idea is simple: instead of just taking the winner axis from RANSAC, we take top-10 candidates, refine them as in ordinary PotSAC and prune them to yield a set of distinctive axes candidates. For the pruning purpose, we check the angle made between each pair of axes—if this angle is below 10° for any pair, then those pairs are assumed redundant, and thus the one with higher cost is discarded. To make the algorithm efficient, we use 10% subsampled surface points for the above steps, after which we run refinement on the survived axes with all surface points.

Fig. 6 shows the modified algorithm outputting 2 axes of which #2 is correct, in contrast to the original PotSAC only yielding the (incorrect) #1 axis. This has allowed complete reassembly of pot A as shown in Fig. 2 at the expense of increased number of pairwise sherd matches from two axes.

3.3. Base sherd and rim detection

The axis of symmetry provides a mean to efficient detect sherds with the base region and the rims.

Base sherd detection We use two sets of information to determine that a sherd contains the base. First, we check the proximity of the sherd with respect to the axis of symmetry. If more than 50 surface points *with* surface normals aligned within 10° from the axis of symmetry are found within 20mm radially from the axis, the sherd is considered a base fragment. Second, we check if there is any sudden change in the sherd's profile curve along the z-axis, which is common for the type of Celadon pots. We form bins every 5mm along the z-axis, and for each bin we compute the mean of the angles between the constituent surface points' normal vectors and the axis of symmetry. If any adjacent bins yield more than 30° difference in the mean surface normal angle, the sherd is also considered a base fragment.

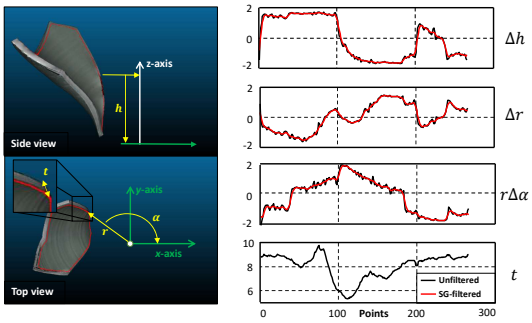

Figure 7. An illustration of our axis-based edge line descriptor. Unfiltered results are computed via finite difference method. The Savitzky-Golay filter is used for smoothing and differentiation followed by a Gaussian filter of width 7 and σ=2.0. Thickness (t) is not filtered as this is sometimes missing in some edge points.

Finally, we align the surface data by the axis of symmetry and project the points onto the xy-plane. We then plot a angular histogram of points that are within 25mm from the axis. If the histogram is evenly spread out, then we regard the sherd as containing the full base. Otherwise, the sherd is flagged as a partial base fragment.

Rim detection For each edge line segment (>25 points) obtained from Sec. 3.1, we check for its consistency in the radial and z-directions— if the radial and vertical standard deviations are less than 3.0mm and 1.5mm respectively, the edge line segment is a rim candidate. We then check if any nearby points along the z-axis have greater radius, which implies the rim is incorrectly segmented. In such case, we drop the edge line from consideration.

3.4. Axis-based edge line descriptor

While previous studies have utilized the axis of symmetry as a physical constraint for incorrect pairwise matching [18], we make one step further and actually encode the information about the axis into each break line (part of the edge line) for efficient matching.

Motivation We note a set of matching break lines from neighboring sherds should ideally meet at the same position from the axis of symmetry. From this observation, we utilize the height (h), radius (r) and angle (α) with respect to the axis of symmetry coordinate system (with the x-axis chosen arbitrarily) as means of providing a description for each of the edge line points (see Fig. 7). Additionally, we incorporate the thickness (t) obtained from Sec. 3.

Need for the derivatives There are two issues with directly using above metrics for matching. First, h and α are computed with respect to some reference defined in each fragment's coordinate system which is almost always different from each other. Second, the absolute value of r can be unreliable for small fragments with high uncertainty in axis translation (see [7] for an illustration). For these reasons, we utilize their derivatives except for t.

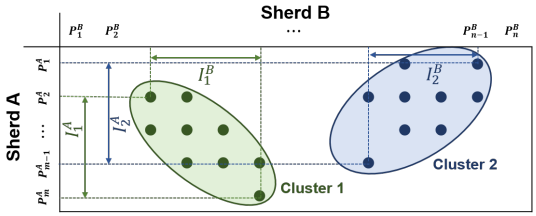

Figure 8. Our LCS matching scheme detects multiple intervals of potential matches between two sherds (<10s for 3160 pairs)

Edge line smoothing Due to noise along the edge lines, simply applying a naive differention technique such as finite differences results in noisy features as shown in Fig. 7. Hence, we apply the Savitzky-Golay digitial differentiator (S-G method) [15] using 7 points, wrapped with a Gaussian filter of width 7 and σ=2.0 to obtain smooth edges.

Descriptor definition Finally, our axis-based descriptor for the edge line point $\mathbf{p}_j \in \mathbb{R}^3$ are defined as

$$\mathbf{f}(\mathbf{p}_j) := [\Delta h(\mathbf{p}_j), \Delta r(\mathbf{p}_j), r\Delta\alpha(\mathbf{p}_j), t(\mathbf{p}_j)]^\top, \quad (1)$$

where Δ involves finite differentiation. (Note r is multiplied to $\Delta\alpha$ to get geometric tangential distance.)

Above can encode all geometric changes regarding each edge line, and it has the benefit of not having to refer to the original point cloud (like in [18]) when checking the axis of symmetry-derived constraints are satisfied.

4. Pairwise matching

Once the geometric edge line descriptors are extracted, we search for pairwise matches across all edge lines in 2 steps: descriptor matching followed by match refinement.

4.1. Descriptor matching

We first match pairs of edge lines by using the longest common subsequence (LCS) algorithm (see [7]). If we denote the matched pair of sherds as A and B respectively, running the algorithm outputs several clusters (known as intervals) of potential matching regions (see Fig. 8). We define this interval as I_k^{AB}, where k is the interval index.

Addressing ambiguities There are 2 folds of ambiguities triggered by the sign ambiguity of the symmetric axis. To account for this, we match each pair of edge lines twice by inverting the descriptor of one edge line.

Rim constraint If the matched interval contains a rim segment, we determine the match is false and discard it.

4.2. Refining matches

While the above descriptor provides useful cues for finding initial correspondences, they are inevitably prone to errors from axis estimation. To refine individual matches, we run iterative closest point (ICP) on the initial pairs of edge lines. The ICP algorithm comprises two stages: correspondence formation followed by correspondence minimization. These steps are repeated until function tolerance is reached.

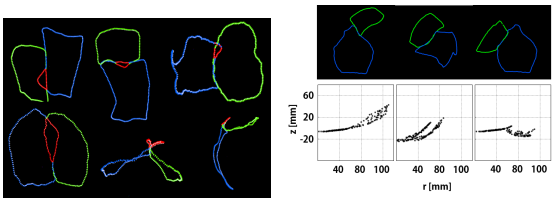

(a) 3D break line overlap test (b) Axis profile curve check

Figure 9. Geometric verification filters 2 cases (a) physically unrealistic overlaps between sherds and (b) non-smooth profile curves.

Forming correspondences In the very first iteration, correspondences are acquired from descriptor matching, and for later iterations, each pair is formed when both points are the closest to (and within 20mm from) each other (i.e. a 1-to-1 relationship) and their normals are within 30°.

Minimizing correspondence distances In the second step, we iteratively find the transformation matrices of the sherds which minimize the geometric distance between the pairs of correspondences while promoting rim segments to maintain consistent radius r and height z.

We define the transformation of sherd A as $\mathtt{T}^A$, which consists of rotation $\mathtt{R}^A \in SO(3)$ and translation $\mathbf{t}^A \in \mathbb{R}^3$ If use the notation (i, j) to denote the correspondence between the i-th edge line point of sherd A ($\mathbf{p}_i^A \in \mathbb{R}^3$) and the j-th edge line point of sherd B ($\mathbf{p}_j^B \in \mathbb{R}^3$), the correspondence distance term can be expressed as $d_{ij}(\mathtt{T}^A, \mathtt{T}^B) := d(\mathbf{p}_i^A, \hat{\mathbf{n}}_i^A, \mathbf{p}_j^B, \hat{\mathbf{n}}_j^B, \mathtt{T}^A, \mathtt{T}^B)$ the correspondence normal deviation term as $e_{ij}(\mathtt{T}^A, \mathtt{T}^B) := e(\hat{\mathbf{n}}_i^A, \hat{\mathbf{n}}_j^B, \mathtt{T}^A, \mathtt{T}^B)$ and the rim consistency term as $g_i(\mathtt{T}^A, r, h) := g(\mathbf{p}_i^A, \mathtt{T}^A, r, h)$. We essentially solve

$$\min_{\mathtt{T}^A, \mathtt{T}^B, r, h} \sum_{(i,j)\in\Omega_{AB}} \rho_d(d_{ij}^2(\mathtt{T}^A, \mathtt{T}^B)) + \lambda\rho_e(e_{ij}^2(\mathtt{T}^A, \mathtt{T}^B)) + \nu \sum_{E\in A,B} \sum_{i\in\Psi_E} \rho_g(g_i^2(\mathtt{T}^E, r, h)) \quad (2)$$

where ρ_d, ρ_e and ρ_g are robust kernels to suppress outlier correspondences, Ω_{AB} is the set of edge line correspondences between sherds A and B, Ψ_E is the set of edge line points classified as rim in sherd E (A or B). While we solve (2) using the Levenberg-Marquardt (LM) algorithm [2], we use different correspondence distance metrics during optimization for which full details are provided in [7].

4.3. Geometric verification

Above ICP algorithm is deliberately unconstrained to yield better empirical convergence properties. Unfortunately, this leads to many false positive matches, requiring further pruning via geometric verification. Similar to [18], we use two tests, detecting an overlapped region between the pair of sherds and checking the axis profile curve. Some examples are shown in Fig. 9 (see [7] for implementation).

5. Incremental sherd registration

We now illustrate the sherd registration module in Fig. 4. We will assume one or more sherds are reassembled in advance, forming a set-of-sherds $\{C\}$.

5.1. Sherd registration

When registering a new sherd (denoted as sherd D) to the reassembled sherds $\{C\}$, we align the coordinates by the sherd C's axis of symmetry (defined as the z-axis without loss of generality) and keep it fixed. We then adjust sherd D's pose ($\mathtt{T}^D$) to align sherd D to sherd C (or sherds $\{C\}$) considering i) the closeness of the edge line matches between sherd D and sherds $\{C\}$ in terms of 3D points and their surface normals, ii) the consistency of the rim in terms of radius r and height z, and iii) the consistency of the symmetric-axis between $\{C\}$ and D. Noting the notations from (2), we essentially solve

$$\min_{\mathtt{T}^D} \sum_{E\in\{C\}} \sum_{(i,j)\in\Omega_{DE}} \rho_d(d_{ij}^2(\mathtt{T}^D,\mathtt{T}^E)) + \lambda\rho_e(e_{ij}^2(\mathtt{T}^D,\mathtt{T}^E)) + \mu \sum_{i\in\Omega_D} \rho_f(f_i^2(\mathtt{T}^D)) + \nu \sum_{i\in\Psi_D} \rho_g(g_i^2(\mathtt{T}^D,r,h)) \quad (3)$$

where Ω_D is the set of edge line points in sherd D, Ψ_D is a subset of Ω_D classified as rim, and f_i is a measure of the axial consistency in sherd D. Specifically, f_i is the extended Cao and Mumford's objective proposed in eq. (9) of [6], which is essentially a function of the edge line point $\mathbf{p}_i^D$, its normal $\hat{\mathbf{n}}_i^D$ and the axis of symmetry (represented by the axis direction $\hat{\mathbf{v}}$ and the axis offset $\mathbf{u}$ in [6].) Unlike in [6] where the objective is used to adjust the axis of symmetry given fixed surface points and normals, we transform each edge line point and its normal as $\mathtt{R}^D\mathbf{p}_i^D + \mathbf{t}^D$ and $\mathtt{R}^D\hat{\mathbf{n}}_i^D$ respectively under fixed symmetric axis ($\hat{\mathbf{v}} = [0,0,1]^\top$, $\mathbf{u} = \mathbf{0}$). We again utilize the ICP algorithm (i.e. the correspondences are updated every iteration) as in Sec. 4.2, and implementation details are provided in [7].

5.2. Priority list

Above registration step yields a set of pairwise matches between the break lines from 2 or more sherds. We then calculate each pair's score based on the number of inliers from which we decide the ranking of pairs.

Adjusted number of inliers From these, we can calculate the number of inlier correspondences (P), which is defined as pairs with less than 1.5 mm. This number is then multiplied by the factor of proportion of overlapping axis profile curve (Q) to yield $(1+Q)P$ as the adjusted number of inliers. For instance, if a sherd C and sherd D have 100 inlier matches, and they share 70% of the overlap in the profile curve, then the adjusted number of inliers is 170.

5.3. Batch sherd alignment

After a priority list ranking is decided, we further refine some of the higher ranked registration results ($k \times b$ candidates using our beam search in Sec. 5.4) by allowing previously re-assembled sherds to move as well. If we suppose now sherd D becomes part of the set of reassembled sherds $\{C\}$, then by noting notations from (2) and (3), we solve

$$\min_{\{\mathtt{T}^C\},r,h} \sum_{(E,F)\in\Omega_{\{C\}}} \sum_{(i,j)\in\Omega_{EF}} \Big(\rho_d(d_{ij}^2(\mathtt{T}^E,\mathtt{T}^F)) + \lambda\rho_e(e_{ij}^2(\mathtt{T}^E,\mathtt{T}^F))\Big) + \sum_{F\in\Omega_{\{C\}}} \Big(\mu \sum_{i\in\Omega_F} \rho_f(f_i^2(\mathtt{T}^F)) + \nu \sum_{i\in\Psi_F} \rho_g(g_i^2(\mathtt{T}^F,r,h))\Big) \quad (4)$$

where (E, F) denote a pair of sherds in set of sherd pairs $\Omega_{\{C\}}$. (Note $\mathtt{T}^E$ and $\mathtt{T}^F$ are members of the set $\{\mathtt{T}^C\}$.) As in Sec. 5.1, we utilize the ICP algorithm to update correspondences via alternation (see [7]).

5.4. Multi-root beam search

We use beam search to explore multitudes of potential reassembly paths. In each iteration, we make b branches from each of the current branches (initially set to 1) and filter k top-ranked beams to bring to the next iteration. Furthermore, to restore multiple pots from the mixed piles of sherds, we utilize multiple roots in each *state* of the beam search (see [7]). This allows efficient matching as each sherd can only be registered to one root per state.

Merging redundant permutations In each beam search iteration, some paths can end up with same reconstruction (with different reassembly order). We consistently check for these and merge such redundant beams.

Estimating initial number of pots In order to run the multi-root beam search framework in Fig. 4, we need to set the number of roots for reassembling pots (which is ideally equal to the number of pots). We achieve this by first gathering a set of sherds with the base region from Sec. 3.3, merging all broken bases and using this number with the number of full (unbroken) bases for initiating the incremental sherd registration process. The merging process involves iteratively selecting an unmerged partial base fragment as root (for incremental beam search) and reassembling all possible pieces until all partial base fragments are reassembled.

6. Experimental results

We carried out experiments to observe the performance of our pipeline under various conditions. The optimization settings and PC environment can be found in [7].

Datasets We used total of 80 fragments from 5 different pots. Pots A and B are actual ancient pots estimated to have been made between the 14–16th century, and Pots C, D and

Pot ID (# sherds)		A (8)	B (9)	C (4)	D (28)	E (31)	A+B (17)	A+B+C (21)	D+E (59)	All (80)
# base sherds (detected / actual)		1 / 1	1 / 1	1 /1	3 / 3	4 / 4	2 / 2	3 / 3	7 / 7	10 / 10
# rim sherds (detected / actual)		5 / 6	6 / 7	2 / 3	1 / 1	0 / 1	11 / 13	13 / 16	1 / 2	14 / 18
# initial pairwise matches		72	98	51	1742	1063	331	483	4715	6431
Preprocessing runtime (min.)		(3.9)	(3.4)	(10.9)	(47.8)	(37.2)	(7.3)	(18.1)	(85.0)	(103.0)
[b=3, k=5]	Accuracy	8 / 8	9 / 9	4 / 4	22 / 28	19 / 31	15 / 17	19 / 21	27 / 59	43 / 80
	Runtime (min.)	(0.2)	(0.2)	(0.1)	(22.5)	(17.0)	(1.1)	(1.9)	(82.3)	(167.5)
[b=5, k=10]	Accuracy	8 / 8	9 / 9	4 / 4	23 / 28	26 / 31	17 / 17	21 / 21	36 / 59	54 / 80
	Runtime (min.)	(0.4)	(0.4)	(0.1)	(49.7)	(32.8)	(2.8)	(3.7)	(210.2)	(256.8)
[b=10, k=20]	Accuracy	8 / 8	9 / 9	4 / 4	24 / 28	24 / 31	17 / 17	21 / 21	48 / 59	66 / 80
	Runtime (min.)	(0.9)	(1.2)	(0.3)	(127.4)	(172.6)	(4.7)	(8.2)	(440.8)	(592.4)

Table 2. Reassembly results on our data. Pot IDs are assigned in ascending order of difficulty. Data preprocessing was run on a slower PC.

[b=3, k=5]	Baseline	w/o beam search	w/o rim	w/o thickness
# initial matches	483	483	634	943
Accuracy	19/21	11/21	18/21	18/21

Table 3. Ablation study of different components proposed in this work (results from the A+B+C multi-pot reassembly setting).

E are modern pots deliberately broken for the purpose of this task. Each pot was scanned with a Creaform GoSCAN 20 at maximum resolution of 0.1mm. The output is a triangulated mesh, but we only utilized the point cloud data for our pipeline. (mesh was used for visualization only.)

We omitted some very small fragments comprising $<$50 points in the respective surface edge lines (i.e. perimeter $\approx$ 9cm), removing 1 piece in pot C, 3 in pot D and 4 in pot E.

Generating ground truth We were provided with reconstructed pot images with each piece labelled by a group of restoration experts. We used these to manually place sherds in correct locations using CloudCompare, and used this to perform ICP using the fracture surfaces between individual sherds to obtain a set of accurate reassembly models (see [7]). Then, for each pot, we recorded the relative transformation ($\mathtt{T}^E$) of each sherd E from the same pot with respect to the base fragment's coordinates.

Counting success For each reconstruction result, we obtained the transformation of each sherd relative to its constituent base fragment's coordinates and compared it to the semi-ground truth data obtained from above. The threshold values for success are 30° for 3D rotation (not the axis deviation) and 20mm for translation.

6.1. Evaluation of our approach

We tested our algorithm under various settings, namely switching between single pot and multi-pot environments and varying the number of branches (b) and beams (k).

As shown in Table 2, our method shows stable performance across all tested beam search settings for the single pot reassembly cases. For the multi-pot setting, beam search with more branches (b) and ranks (k) overall increases the number of successfully reassembled fragments as predicted, largely due to the increased number of trials allowing the pipeline yield a better solution. Interestingly, in some cases it is the opposite, and we think this is potentially due to earlier-rejected beam paths surviving for larger k and coming back later to negatively influence the result.

While a direct comparison with Son et al.'s method (31/48 sherds reassembled in 648 minutes) is difficult due to difference in datasets, we show over 17.9% improvement in reassembly accuracy with 32 more fragments.

Ablation study We also checked the performance gain brought by the individual components we proposed in this work. Table 3 shows beam search is mandatory for successful reassembly and the new set of constraints using the rim and thickness information helps to reduce the number of initial pairwise matches by 30–50%.

Note on hyperparameters While we made efforts to build a generic pipeline, some hyperparameters need to be tuned correctly. These include parameters for edge line extraction, the threshold for checking sherd overlaps and ICP weights and kernel widths (see [7] for details).

7. Conclusions

In this work, we have addressed the problem of virtually reassembling axially symmetric pots from 3D scanned fragments. We empirically showed a global reassembly pipeline is sensitive to inaccurate pairwise feature matches between pot sherds arising from ambiguous geometric cues. In addressing this intrinsic difficulty, we formed a strong connection between structure-from-motion (SfM) and pot reassembly, inspiring us to utilize incremental registration widely adopted in SfM. Additionally, we proposed several major extensions, i) an axis-based geometric feature descriptor for matching, ii) adoption of beam search to maintain a pool of registration possibilities, and iii) multiple root nodes in each beam state to reduce the number of false matches in reassembling multiple pots simultaneously. We also showed rim and thickness information help in reducing false matches. Through experiments on a larger number of pot fragments and pot types than previously reported in the literature, we showed our method achieves significant improvement in reassembly accuracy over the state-of-the-art.

Acknowledgement This work was supported by South Korea's Ministry of Culture, Sports and Tourism (MCST) and the Korea Creative Content Agency (KOCCA) through the Culture Technology (CT) Research & Development Program (R2018020101).

References

[1] Sameer Agarwal, Yasutaka Furukawa, Noah Snavely, Ian Simon, Brian Curless, Steven M. Seitz, and Richard Szeliski. Building rome in a day. *Commun. ACM*, 54(10):105–112, 2011. 2

[2] Sameer Agarwal, Keir Mierle, and Others. Ceres solver. http://ceres-solver.org. 6

[3] Yan Cao and David Mumford. Geometric structure estimation of axially symmetric pots from small fragments. In *Proceedings of Signal Processing, Pattern Recognition, and Applications*, 2002. 2, 4

[4] R. Hartley, J. Trumpf, Yuchao Dai, and Hongdong Li. Rotation averaging. *International Journal of Computer Vision*, 103:267–305, 2012. 3

[5] Richard Hartley and Andrew Zisserman. *Multiple View Geometry in Computer Vision*. Cambridge University Press, New York, NY, USA, 2 edition, 2003. 3

[6] Je Hyeong Hong, Young Min Kim, Koang-Chul Wi, and Jinwook Kim. Potsac: A robust axis estimator for axially symmetric pot fragments. In *Proceedings of the IEEE/CVF International Conference on Computer Vision (ICCV) Workshops*, Oct 2019. 4, 7

[7] Je Hyeong Hong*, Seong Jong Yoo*, Muhammad Zeeshan Arshard, Young Min Kim, and Jinwook Kim. Supplementary document for structure-from-sherds: Incremental 3d reassembly of axially symmetric pots from unordered and mixed fragment collections. https://github.com/SeongJong-Yoo/structure-from-sherds, 2021. 4, 5, 6, 7, 8

[8] Qi-Xing Huang, Simon Flöry, Natasha Gelfand, Michael Hofer, and Helmut Pottmann. Reassembling fractured objects by geometric matching. *ACM Trans. Graph.*, 25(3):569–578, July 2006. 2, 3

[9] M. Leordeanu and M. Hebert. A spectral technique for correspondence problems using pairwise constraints. In *Tenth IEEE International Conference on Computer Vision (ICCV'05) Volume 1*, volume 2, pages 1482–1489 Vol. 2, 2005. 3

[10] David G. Lowe. Distinctive image features from scale-invariant keypoints. *Int. J. Comput. Vision*, 60(2):91–110, Nov. 2004. 3

[11] Hubert Mara and Robert Sablatnig. Orientation of fragments of rotationally symmetrical 3d-shapes for archaeological documentation. In *Proceedings of the Third International Symposium on 3D Data Processing, Visualization, and Transmission (3DPVT'06)*, 3DPVT '06, pages 1064–1071, Washington, DC, USA, 2006. IEEE Computer Society. 2, 4

[12] J. C. McBride and B. B. Kimia. Archaeological fragment reconstruction using curve-matching. In *2003 Conference on Computer Vision and Pattern Recognition Workshop*, volume 1, pages 3–3, 2003. 2

[13] Georgios Papaioannou, Tobias Schreck, Anthousis Andreadis, Pavlos Mavridis, Robert Gregor, Ivan Sipiran, and Konstantinos Vardis. From reassembly to object completion: A complete systems pipeline. *J. Comput. Cult. Herit.*, 10(2), Mar. 2017. 1

[14] Helmut Pottmann, Martin Peternell, and Bahram Ravani. An introduction to line geometry with applications. *Computer-Aided Design*, 31(1):3–16, 1999. 2

[15] A. Savitzky and M. J. E. Golay. Smoothing and differentiation of data by simplified least squares procedures. *Analytical Chemistry*, 36:1627–1639, 1964. 6

[16] Johannes Lutz Schönberger and Jan-Michael Frahm. Structure-from-Motion Revisited. In *Conference on Computer Vision and Pattern Recognition (CVPR)*, 2016. 2, 3

[17] Noah Snavely, Steven M. Seitz, and Richard Szeliski. Photo tourism: Exploring photo collections in 3d. In *ACM SIGGRAPH 2006 Papers*, SIGGRAPH '06, page 835–846, New York, NY, USA, 2006. Association for Computing Machinery. 2

[18] Kilho Son, Eduardo B. Almeida, and David B. Cooper. Axially symmetric 3d pots configuration system using axis of symmetry and break curve. In *IEEE Conference on Computer Vision and Pattern Recognition (CVPR)*, June 2013. 1, 2, 3, 4, 5, 6

[19] A. Willis, X. Orriols, and D. B. Cooper. Accurately estimating sherd 3d surface geometry with application to pot reconstruction. In *Proceedings of the 2003 Conference on Computer Vision and Pattern Recognition Workshop*, volume 1, pages 5–5, June 2003. 2

[20] A. R. Willis and D. B. Cooper. Bayesian assembly of 3d axially symmetric shapes from fragments. In *Proceedings of the 2004 IEEE Computer Society Conference on Computer Vision and Pattern Recognition, 2004. CVPR 2004.*, volume 1, pages I–I, June 2004. 2, 3

[21] Kyle Wilson and Noah Snavely. Robust global translations with 1dsfm. In *Proceedings of the European Conference on Computer Vision (ECCV)*, 2014. 3

[22] C. Wu. Towards linear-time incremental structure from motion. In *2013 International Conference on 3D Vision - 3DV 2013*, pages 127–134, 2013. 2

[23] C. Zach, M. Klopschitz, and M. Pollefeys. Disambiguating visual relations using loop constraints. In *2010 IEEE Computer Society Conference on Computer Vision and Pattern Recognition*, pages 1426–1433, 2010. 3, 4

[24] K. Zhang, W. Yu, M. Manhein, W. Waggenspack, and X. Li. 3d fragment reassembly using integrated template guidance and fracture-region matching. In *2015 IEEE International Conference on Computer Vision (ICCV)*, pages 2138–2146, 2015. 2, 3